International Journal of Energy Research

WILEY

RESEARCH ARTICLE OPEN ACCESS

Power System Global Instability Risk Assessment Framework in the Presence of Renewable Wind Generation

Umair Shahzad

School of Computer Science and Engineering, University of Sunderland, Sunderland, UK

Correspondence: Umair Shahzad (umair.shahzad@sunderland.ac.uk)

Received: 14 April 2026 | **Revised:** 29 May 2026 | **Accepted:** 22 June 2026

Academic Editor: Cheng Du

Keywords: fault | power system | renewable energy | risk | stability | uncertainty | wind

ABSTRACT

As power systems transition toward high renewable penetration, assessing stability through deterministic margins is becoming obsolete due to rising operational uncertainties. This paper develops a novel probabilistic risk-based framework to compute a Global Instability Index, which simultaneously accounts for rotor angle, voltage, and frequency stability under large-scale disturbances. The primary goal of this research is to establish a rigorous and risk-based global instability framework capable of simultaneously assessing distinct stability modes in modern and converter-heavy networks. Using the IEEE 39-bus test system, the study systematically evaluates the impact of increasing wind power penetration from 20% to 80%. Quantitative analysis reveals that the integration of doubly fed induction generator (DFIG)–based wind farms provides a stabilizing effect, lowering the global instability risk by approximately 46.8% at maximum penetration levels. Detailed case studies investigate the influence of shifting generation patterns and load fluctuations, demonstrating that the proposed global index serves as a more robust indicator of system health than conventional single-variable metrics. These findings suggest that modern wind generation, when properly integrated, can effectively mitigate the risks associated with traditional synchronous machine displacement.

1 | Introduction

Since the early 20th century, power system stability has been established as a very substantial component of power system planning and operation [1, 2]. This phenomenon has played a very critical role in most cascading outages and blackouts [3, 4]. As elaborated in Figure 1, there are various kinds of stability in power systems, such as voltage stability, frequency stability, and rotor angle stability [5]. "Rotor angle stability is the ability of synchronous machines in a power system to maintain synchronism when a disturbance is applied [5]. Instability can occur when the angular swing of the generators causes a loss in synchronism. Large-disturbance rotor angle stability, or commonly known as transient stability, deals with the ability of the power system to maintain synchronism when a severe disturbance, such as a three-phase short circuit on a transmission line, is applied. Large-disturbance voltage stability is the ability of a power system to maintain steady voltages after large disturbances occur, such as short-circuit faults. Frequency stability is the ability of a power system to maintain steady frequency after a serious system disturbance causes a considerable discrepancy between generation and demand" [5, 6].

Abbreviations: AGC, automatic generation control; DFIG, doubly fed induction generator; DG, distributed generation; FCT, fault clearing time; IEC, International Electrotechnical Commission; LG, single line to ground; LL, line to line; LLG, line to line to ground; LLL, line to line to line; LVRT, low voltage ride through; MC, Monte Carlo; PMSG, permanent magnet synchronous generator; PMU, phasor measurement unit; PSS, power system stabilizer; PV, photo voltaic; SG, synchronous generator; SMIB, single machine infinite bus; STATCOM, static synchronous compensator; TSA, transient stability assessment; WECC, Western Electricity Coordinating Council.

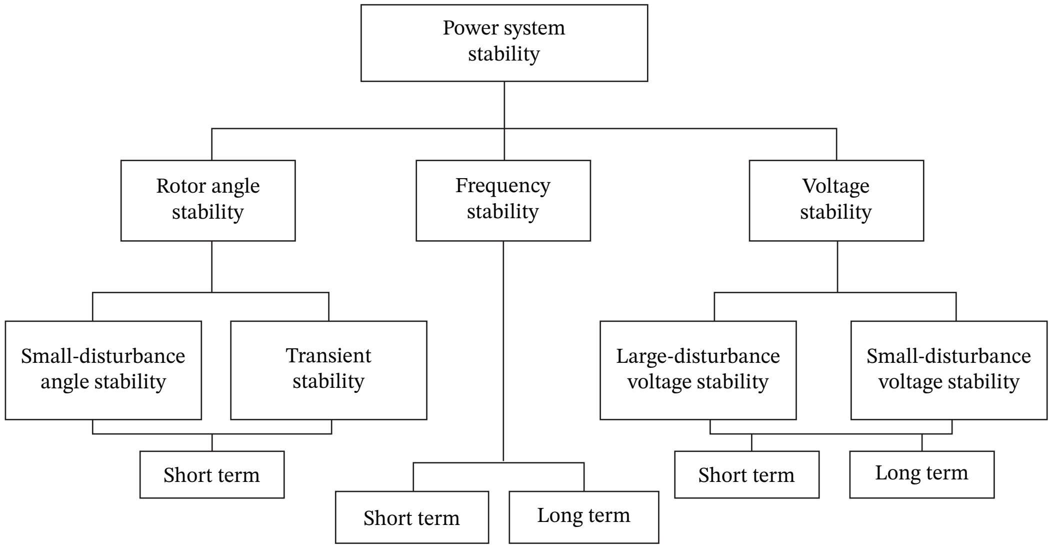

FIGURE 1 | Classification of power system stability.

In traditional power system stability analysis, a deterministic stability limit is used which depends on the worst-case scenario. This confines the reasonable stable operating condition and thus restricts the technical capabilities of the power generation to meet the load demand [7]. Moreover, the deterministic approach for power system stability evaluation does not give any information on the status of the present operating point but only provides information regarding the stability or instability of a current condition of operation [8]. Moreover, with the increasing usage of renewables such as wind and photovoltaics (PVs), in addition to load uncertainties, assessing stability in a deterministic manner is no longer pertinent [9].

Integration of wind energy can result in grid instability issues due to the limitations of wind generation. For instance, wind power is inherently intermittent, variable, and unpredictable. It is not dispatchable and depends on the weather conditions. This means that they can alter unpredictably and cause mismatches between supply and demand. For example, a sudden drop in wind speed can reduce the output of wind turbines, while a spike in demand can create a shortage of power. A significant mismatch between the total generation and demand on the grid can lead to frequency disturbances. Due to the power electronics converter, the system alters its characteristics dynamically.

The prevailing industry practice relies on a deterministic approach for stability assessment [10, 11]. In most situations, the $N-1$ contingency criterion is applied, meaning that system components are removed individually for evaluation. The worst-case scenario is then translated into multiple extreme operating conditions along with several critical contingencies, for which the system must be designed to remain secure. Deterministic stability assessment follows a sequential procedure in which parameters such as load, fault types, and fault locations are predefined, typically based on a worst-case philosophy. Additionally, to ensure that the most severe disturbance is considered, contingency types and their locations are usually specified beforehand. In this framework, contingencies are chosen with some consideration of probability; however, once selected, they are treated as equally likely, and operational limits are established based on their impacts [6]. Although this worst-case methodology has historically been effective, in a competitive environment, utilities must understand the level of risk associated with their criteria so they can adjust service quality according to consumer expectations, that is, acceptable risk levels and corresponding costs. The deterministic approach evaluates only the consequences of contingencies while neglecting their likelihood of occurrence. Even if a contingency has limited consequences, the overall system risk may still be significant if its probability is high. Conversely, if an outage event has an extremely low probability, analyzing such a contingency may lead to economically inefficient operational decisions [6].

Furthermore, since deterministic stability analysis produces a binary outcome (stable or unstable), it does not allow the quantification of instability risk. In practice, the power sector requires knowledge of risk levels to take appropriate actions that enhance the system security. As a result, assessing transient stability through risk-based methods has become an important research direction. With the ongoing transition toward competitive and deregulated electricity markets, utilities are expected to maintain both high reliability and economic efficiency while maximizing the use of the existing infrastructure. Consequently, some operators explore operating regions beyond traditional limits—where the system may be exposed to costly outages—to evaluate whether the associated risks are justified by potential economic gains. In such contexts, probabilistic approaches offer substantial advantages as they account for the stochastic nature of real power systems by incorporating probability distributions of uncertain parameters, thereby providing a more realistic representation of system behavior [6].

While deterministic methods tend to yield highly secure system designs, they fail to capture the inherent uncertainty associated with system conditions and components. In addition to the high costs linked to conventional approaches, a major limitation is that all security issues are treated as having equal risk [12]. Moreover, key uncertainties, such as variations in load and renewable generation, are often ignored. Several studies [13–16] identify probabilistic risk-based stability assessment and the integration of risk into power system planning as important future research areas. Similarly, planning guidelines from various utilities [17–20] advocate the adoption of probabilistic risk-based methods in the near future. The increasing integration of renewable energy sources further amplifies system uncertainty, making probabilistic approaches essential for stability assessment. Such methods [21, 22] are particularly valuable when uncertain parameters are incorporated into system analysis. Therefore, it is crucial to develop risk-based approaches to overcome the limitations of deterministic methods. In line with this objective, the primary aim of this research is to introduce a risk-based global instability index for power systems, taking into account the impact of wind generation. Relevant prior work in power system stability risk assessment is discussed later.

Hamida et al. [23] elaborated some characteristics of the Tunisian power system transient stability. Angular stability is analyzed using the fault clearing time (FCT). Many contingency cases were considered: the outage of the largest generator and loss of load, along with insufficient operation of the power system stabilizer (PSS). Although the work considered different FCTs, only a three-phase fault at a specific line was chosen. Moreover, the integration of any renewable energy source was not part of this work. Papadopoulos and Milanovic [24] proposed a probabilistic framework for power system transient stability assessment (TSA) with high renewable generation penetration. The presented framework enabled the comprehensive calculation of transient stability of power systems with abridged inertia. A major drawback of the work was the ignorance of bus faults and only considering three-phase line faults. Moreover, the impact of different wind technologies and penetration levels was not considered. Agber et al. [25] presented a study of the effects of some important power system parameters on transient stability. The parameters considered for this assessment included fault location, load change, machine damping factor, FCT, and generator synchronous speed. The work only considered three-phase line faults, and the influence of renewable generation integration on transient stability was not studied.

The TSA including wind power intermittency and volatility was proposed in Shi et al. [26]. The kinds of wind turbines considered in this work included the doubly fed induction generator (DFIG) and direct-driven permanent magnet synchronous generator (PMSG). The Monte Carlo (MC) simulation method, joint with two evaluation indices, was tested on the IEEE 39-bus test system and a real China–Jiangxi power network to investigate the impacts of intermittency and volatility of wind. Although the work incorporated the effect of wake effect on transient stability, it only considered a three-phase fault at a specific bus, which was cleared after a preselected time. Miao et al. [27] used a risk-based approach to analyze the transient stability of power networks integrating wind farms. The proposed methodology of transient stability risk assessment was based on the MC method, and eventually, an inclusive risk indicator based on angle and voltage stability was devised. The work only considered three-phase line faults, and the impact of different wind technologies was not studied. In Wang et al. [28], the abridged version of an altered single machine infinite bus (SMIB) system, with a DFIG-based wind farm integration, was analyzed using the transient features of the DFIG–based wind farm in the diverse periods of a fault. The assessment specified that the working of the synchronous generator (SG) can be either enhanced or depreciated with DFIG integration. Only a three-phase fault was considered on a specific line, which cleared after a preselected time.

In Khani et al. [29], the transient and voltage stability with high penetration levels of the diverse distributed generations (DGs) were examined. With each penetration level of DGs, the performance of the power system was analyzed, and the results were equated with the performance of the power network base case (no DG integration). Only specific fault types and fault locations were considered. Zou and Zhou [30] explored the voltage stability of wind power grid integration. Furthermore, static synchronous compensator (STATCOM) and its sizing approach were proposed to enhance the voltage stability of the wind farm integrated grid. The results were obtained for a specific fault and the FCT. An approach for examining short-term voltage stability of power systems incorporating induction motors was proposed in Wang et al. [31]. This approach considered one generator as the reference machine, and the comparative angle difference was considered as a differential variable. Besides, a mathematical approach of differential equation series was devised in the polar coordinates. Meegahapola and Flynn [32] suggested the influence on transient and frequency stability for high wind penetration. DFIG wind generation was used, and sensitivity analysis was conducted for various wind generator loading conditions. The study proved that transient stability evaluation is highly dependent on the fault location in the system. Frequency stability analysis showed that areas with reduced inertia were most impacted by generator outage events. Abdlrahem et al. [33] studied the impact of a large PV plant on the frequency stability of a power network when subjected to small and large disturbances. With the help of automatic generation control (AGC) and phasor measurement unit (PMU) data, the power generation levels of traditional generators were attuned to alleviate the deviations in system frequency. Additionally, the impact of heightened PV penetration was inspected. Only a three-phase fault with a fixed FCT was considered.

In risk-based stability assessment, the risk index is computed quantitatively for each possible contingency and its associated impact (severity) [34]. Some research work has been done in this area. For instance, Miao et al. [27] proposed a methodology to compute transient instability risk index based on angle and voltage instabilities. Although the work considered the probabilistic nature of the FCT, the main drawback was the consideration of predetermined fault locations of lines and associated probabilities. Vittal et al. [35] proposed a methodology to compute the risk of transient instability of an operating point in a power network. The work included various cost parameters to quantify the consequences of the risk.

From the literature review, some significant findings were obtained. Most works on probabilistic large-signal short-term stability dealt with only three phase faults. Although the assumption may be suitable since it is the most severe fault, other faults cannot be ignored as their probabilities are higher and must be included in probabilistic stability assessment. Although various research [27, 36] regarding risk assessment of each of the stability type exist; however, to the best of author's knowledge, there is no research which deals with the significant problem of global system risk encapsulating all three kinds of stability. Moreover, Ma et al. [37] and Xue et al. [38] indicated the need to establish a comprehensive global approach for power system stability incorporating all stabilities: angle, voltage, and frequency. Hasan et al. [11], Li and Zhou [13], and Milanovic [15] indicated that the risk-based stability approach is an open area of research and requires further work. Moreover, the impact of reduced inertia systems (i.e., higher wind penetration) on power system stability is of great implication [39, 40] as the stored energy due to inertia is invaluable under fault condition.

Traditional power system security paradigms rely on decoupled stability assessments, evaluating rotor angle, voltage, and frequency dynamics as isolated phenomena. While this compartmentalization was acceptable in traditional systems dominated by massive synchronous generation, it becomes a critical blind spot in modern low-inertia and converter-dominated networks. In high-penetration renewable grids, these distinct stability modes are deeply coupled through fast-acting converter control loops and network topologies. For instance, a severe localized voltage drop immediately alters the electrical power output of nearby SGs, inducing rapid rotor angle acceleration. Simultaneously, the resulting power mismatch triggers systemic frequency deviations, aggravated by the reduced kinetic energy storage of the displaced conventional units. Relying solely on conventional single-variable metrics (such as isolated transient stability indices or independent bus voltage security margins) fails to capture these complex cross-domain interactions. An operator tracking a single dimension may observe a secure rotor angle profile while remaining oblivious to an imminent coupled voltage–frequency collapse. Therefore, justifying a holistic framework requires moving beyond disjointed safety thresholds. This paper bridges this gap by integrating these highly interdependent phenomena into a single probabilistic risk framework, establishing a multidimensional safety envelope that reflects the true composite health of the grid. Thus, the key contribution and novelty of this paper is to present a probabilistic approach for power system large-disturbance global instability risk assessment in the presence of renewable wind generation, incorporating all kinds of stability (angle, voltage, and frequency) [41].

The rest of the paper is organized as follows: Section 2 discusses the background and mathematical formulation of the risk-based global instability index for a large disturbance. Section 3 elaborates on the procedure for computing this index. Section 4 discusses the modeling approach for SGs and DFIGs. Section 5 discusses case studies and associated simulations on the IEEE 39-bus test system. Section 6 presents the results and associated discussion. Finally, Section 7 concludes the paper with suggested future research directions.

2 | Risk-Based Global Instability Index: Background and Mathematical Formulation

Section 2 will discuss the background, theory, and mathematical formulation of the risk-based global instability index. Figure 2 shows the flowchart outlining the procedure to evaluate the risk-based global instability index, G. Based on this flowchart, the global instability risk index can be defined as the maximum value of the risk index from a set of risk indices describing angle, voltage, and frequency instability. As this is a global index, it will eventually be useful to assess overall instability, which allows to tackle the worst cases of faults and cascading outages. The global risk index evaluation consists of the following main steps: (1) determining component outage models, (2) selecting system states and calculating their probabilities, (3) evaluating the consequences of selected system states, (4) calculating the angle, voltage, and frequency instability risk indices, and (5) eventually computing the global risk index.

The product of probability of an unexpected event and its consequence is known as risk, which is mathematically defined as Equation (1) [12, 42]. The reader can refer to Li et al. [43] and Shahzad and Asgarpoor [44] for a detailed theory on risk and its

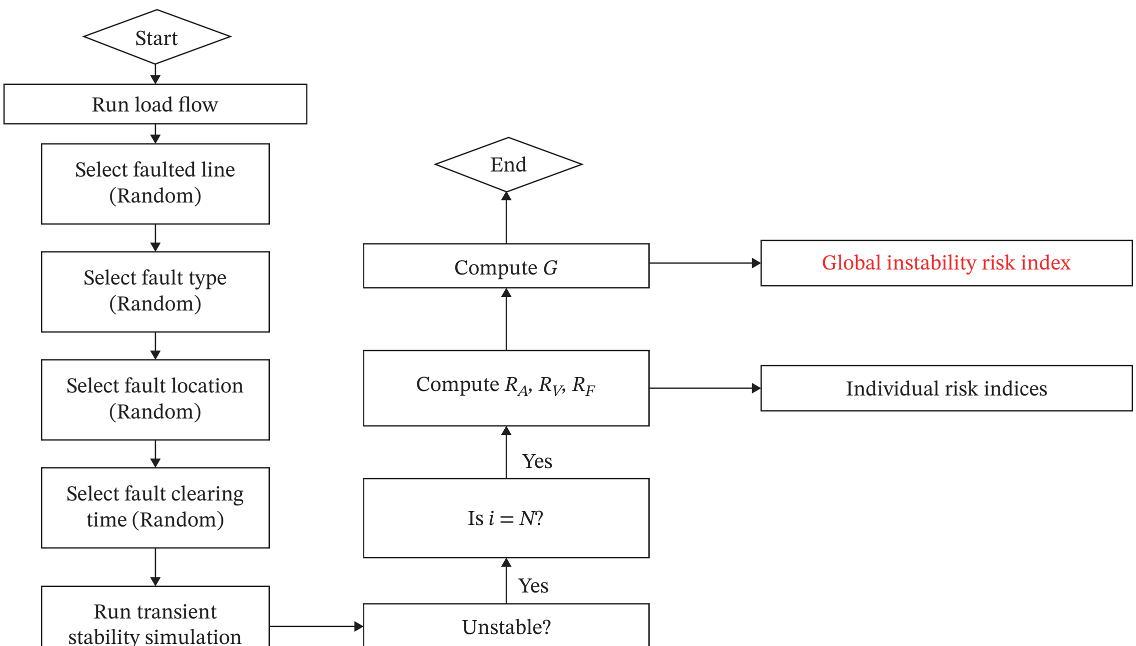

FIGURE 2 | Procedure to compute global instability risk index (G).

applications in power systems.

$$\text{Risk}\left(X_{t,f}\right) = \sum_i \Pr(E_i)\left(\sum_j \Pr\left(X_{t,j}|X_{t,f}\right) \times \text{Sev}\left(E_i, X_{t,j}\right)\right), \tag{1}$$

where $X_{t,f}$ is the forecasted operating condition at time t; $X_{t,j}$ is the j^{th} possible loading level; $\Pr(X_{t,j}|X_{t,f})$ is the probability of $X_{t,j}$ given $X_{t,f}$ has occurred, which is obtained using a probability distribution for the possible load levels; E_i is the i^{th} contingency and $\Pr(E_i)$ is its probability; $\text{Sev}(E_i, X_{t,j})$ quantifies the impact of E_i occurring under the j^{th} possible operating condition.

Let $R_A(X_{t,f})$ (or R_A for simplicity) be the risk index for angle instability, that is,

$$R_A\left(X_{t,f}\right) = \sum_{i=1}^{N} \Pr(F_i)\left(\sum_j P\left(X_{t,j}|X_{t,f}\right) \times \text{Sev}\left(A_i, X_{t,j}\right)\right), \tag{2}$$

where $\Pr(F_i)$ is given by:

$$\Pr(F_i) = \Pr(F_{\text{oi}}) \times \Pr(F_{\text{Li}}) \times \Pr(F_{\text{Ti}}). \tag{3}$$

$\Pr(F_{\text{oi}})$, $\Pr(F_{\text{Li}})$, and $\Pr(F_{\text{Ti}})$ denote the probability of fault occurrence, fault location, and fault type, respectively, for the i^{th} MC sample. It is assumed that fault can occur on any line on the system and at any point along the line; hence,

$$\Pr(F_{\text{oi}}) = \frac{1}{N_L}, \tag{4}$$

where N_L denotes total number of lines in the power system.

$$\Pr(F_{\text{Li}}) = \frac{1}{100}. \tag{5}$$

$\Pr(F_{\text{Ti}})$ denotes probability of fault type and will be chosen based on discrete distribution as described in Section 3.

$X_{t,f}$ is the forecasted operating condition at time t; $X_{t,j}$ is the j^{th} possible loading level; $\Pr(X_{t,j}|X_{t,f})$ is the probability of this condition; F_i is the i^{th} fault and $\Pr(F_i)$ is its probability; $\text{Sev}(A_i, X_{t,j})$ quantifies the impact of F_i occurring under the j^{th} possible operating condition (for angle instability). It is assumed that $\text{Sev}(A_i, X_{t,j})$ denotes the severity under peak loading condition. For simplicity, it is represented by $\text{Sev}(A_i)$ in the following equation:

$$\text{Sev}(A_i) = \begin{cases} |\text{TSI}_i|, \text{ if } \text{TSI}_i < 0 \\ 0, \text{ if } \text{TSI}_i > 0 \end{cases}, \tag{6}$$

where TSI_i is the angle stability index, that is,

$$\text{TSI}_i = \frac{360 - \delta\,\text{max}i}{360 + \delta\,\text{max}i}, -1 < \text{TSI}_i < 1, \tag{7}$$

where $\delta_{\max i}$ is the maximum angle difference between any two SGs after the fault at i^{th} line. A negative TSI_i indicates an unstable system. As an illustration, $\delta_{\max}$ is indicated on Figure 3 for a three-phase short circuit fault at Line 16–17 (line between bus 16 and bus 17) for the IEEE 39-bus system. The fault occurs at time $t = 1.0$ s and clears at time $t = 1.1$ s.

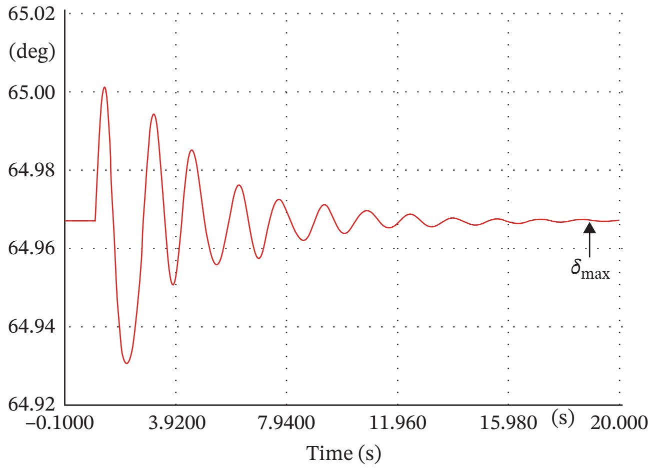

FIGURE 3 | Illustration of maximum rotor angle difference $\delta_{\max}$.

Let $R_V(X_{t,f})$ (or R_V for simplicity) be the risk index for voltage instability, that is,

$$R_V\left(X_{t,f}\right) = \sum_{i=1}^{N}\sum_{k=1}^{N_b} \Pr(F_i)\left(\sum_j P\left(X_{t,j}|X_{t,f}\right) \times \text{Sev}\left(V_i, X_{t,j}\right)\right). \tag{8}$$

$\text{Sev}(V_i, X_{t,j})$ quantifies the impact of F_i occurring under the j^{th} possible operating condition (for voltage instability). It is assumed that $\text{Sev}(V_i, X_{t,j})$ denotes the severity under peak loading condition. For simplicity, it is represented by $\text{Sev}(V_i)$in the following equation:

$$\text{Sev}(V_i) = \begin{cases} |V_{\text{dk}}|, \text{ if } |V_{\text{dk}}| > 5\% \\ 0, \text{ if } |V_{\text{dk}}| < 5\% \end{cases} \forall k \in N_b\ . \tag{9}$$

V_{dk} indicates the voltage deviation for bus k, that is,

$$V_{\text{dk}} = V_{\text{rated}} - V_k, \tag{10}$$

where V_{rated} is the nominal voltage (1 p.u.) of each bus; V_k is the postfault steady-state voltage at k^{th} bus; N_b denotes total number of buses in the system; N denotes number of MC samples.

As an illustration, V_k (for Bus 20 of IEEE 39-bus system) is marked in Figure 4 for a three-phase short circuit fault at Line 16–17. The fault occurs at time $t = 1.0$ s and clears at time $t = 1.1$ s.

Let $R_F(X_{t,f})$ (or R_F for simplicity) be the risk index for frequency instability, that is,

$$R_F\left(X_{t,f}\right) = \sum_{i=1}^{N}\sum_{k=1}^{N_g} \Pr(F_i)\left(\sum_j P\left(X_{t,j}|X_{t,f}\right) \times \text{Sev}\left(F_i, X_{t,j}\right)\right). \tag{11}$$

$\text{Sev}(F_i, X_{t,j})$ quantifies the impact of F_i occurring under the j^{th} possible operating condition (for frequency instability). It is assumed that $\text{Sev}(F_i, X_{t,j})$ denotes the severity under peak loading condition. For simplicity, it is represented by $\text{Sev}(F_i)$ in the following equation:

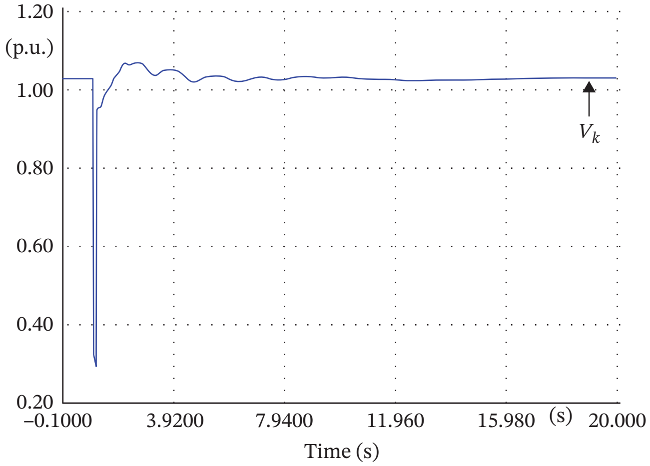

FIGURE 4 | Illustration of postfault steady state voltage V_k.

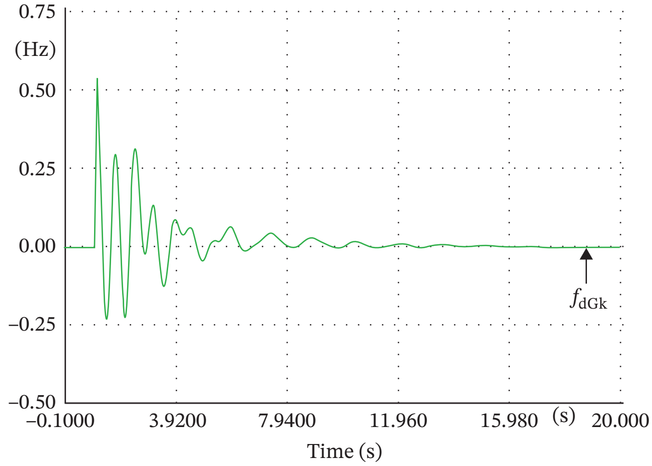

FIGURE 5 | Illustration of postfault electrical frequency deviation f_{dGk}.

$$\mathrm{Sev}(F_i) = \begin{cases} |f_{\mathrm{dGk}}|, \text{ if } |f_{\mathrm{dGk}}| > 0.5\,\mathrm{Hz} \\ 0, \text{ if } |f_{\mathrm{dGk}}| < 0.5\,\mathrm{Hz} \end{cases} \forall G_k \in N_g. \tag{12}$$

f_{dGk} denotes the postfault deviation of frequency from nominal frequency (60 Hz) for k^{th} generator (G_k) and N_g denotes total number of generators in the system. To illustrate, f_{dGk} is marked in Figure 5 for a three-phase short circuit fault at Line 16–17 (IEEE 39-bus system). The fault occurs at time $t = 1.0$ s and clears at time $t = 1.1$ s.

It must be noted that the individual risk index is inherently normalized because the severity/impact functions are formulated on bounded, standardized scales derived from standard engineering limits. Traditional composite indices often synthesize multidimensional risks using linear-weighted aggregation as follows:

$$G_{\mathrm{weighted}} = w_1 R_{\mathrm{AM}} + w_2 R_{\mathrm{VM}} + w_3 R_{\mathrm{FM}}.$$

However, selecting weighting factors (w_1, w_2, and w_3) introduces subjective bias and risks masking critical system vulnerabilities (e.g., a catastrophic frequency collapse could be mathematically obscured by a highly stable voltage profile). To eliminate this ambiguity and ensure operational security, this framework avoids arbitrary weighting factors by employing a critical envelope (worst case) formulation. Therefore, the statistical mean of each individual risk metric across all N MC samples is computed. By utilizing a maximum operator instead of fractional weighting parameters, the index preserves the visibility of the most critical threat facing the network, ensuring that grid operators plan defenses against the weakest link in the system's stability chain.

Let R_{AM}, R_{VM}, and R_{FM} be the mean (average) values of R_A, R_V, and R_F, respectively. Mathematically,

$$R_{\mathrm{AM}} = \frac{\sum_{n=1}^{N} R_{\mathrm{An}}}{N}, \tag{13}$$

$$R_{\mathrm{VM}} = \frac{\sum_{n=1}^{N} R_{\mathrm{Vn}}}{N}, \tag{14}$$

$$R_{\mathrm{FM}} = \frac{\sum_{n=1}^{N} R_{\mathrm{Fn}}}{N}, \tag{15}$$

where $R_{\mathrm{An}}, R_{\mathrm{Vn}}, R_{\mathrm{Fn}}$ is the value of R_A, R_V, and R_F, for n^{th} MC sample, respectively, and N is the total number of MC samples.

The Global Instability Index G is then formulated as the maximum absolute risk among the three primary stability dimensions. Let G be the global instability risk index, that is,

$$G = \max\{R_{\mathrm{AM}}, R_{\mathrm{VM}}, R_{\mathrm{FM}}\}. \tag{16}$$

Equally foundational to this formulation is the deliberate assignment of equal structural significance to each stability domain within the extreme-event envelope. In conventional security metrics, varying weighting coefficients are often introduced to reflect the perceived hierarchical priority of one stability mode over another. However, in low-inertia converter-dominated networks, prioritizing any single domain is physically unjustifiable due to the highly fluid and interdependent nature of modern grid failure mechanisms. A severe disturbance can initiate an instantaneous voltage collapse at weak buses, trigger an immediate cascading rotor angle divergence across adjacent synchronous groups, or precipitate a rapid frequency nadir due to diminished system inertia. Because each of these phenomena independently possesses the capacity to induce complete systemic blackouts, they represent equal existential risks to the operational integrity of the power system. Assigning equal structural weightage across all normalized indices ensures that the framework remains completely objective, mathematically rigorous, and agnostic to a priori assumptions about which failure mode will manifest first. This egalitarian structural design ensures that an escalation of risk in any single domain is treated with identical gravity, providing a true and unbiased reflection of multidimensional system vulnerability.

3 | Computation Procedure

"There are several random variables which must be considered in the probabilistic analysis of transient stability of power systems. Some of these include the kind of fault, location of fault, and clearing time of fault [6, 45]. Appropriate density functions were used to model these variables. Regarding faults, a general practice is to incorporate three-phase (LLL), double-line-to-ground (LLG), line-to-line (LL), and single-line-to-ground (LG) faults [6, 45]. A discrete density function is usually used to model the fault type. Based on historic network statistics, the norm is to choose the probability of LLL, LLG, LL, and LG short circuits as 0.05, 0.1, 0.15, and 0.7, respectively [6, 45, 46]. The probability distribution of fault location on a transmission line is usually assumed to be uniform, that is, the fault occurs with equal probability at any point along any line of the test network [24, 47]. A Gaussian distribution is generally used to model the FCT [6, 24, 47]. The fault is applied at 1 s, and it is cleared after a mean time of 0.3 s and standard deviation of 0.005 s (based on the normal distribution). The detailed computation procedure is shown in Figure 6. In the first step, load flow is run on the base case under normal conditions, that is, without any fault. Then, a random line is selected for fault. The line is selected based on uniform distribution, as described above. Then, the fault type and fault location on the line are selected. The fault was then cleared based on the FCT Normal distribution. The transient stability time domain simulation is done for 20 s (which is usually the time for a large disturbance power system stability study for a relatively large interconnected system). After making sure that there are enough samples for convergence, risk indices for the angle, voltage, and frequency are computed. Eventually, a global instability risk index was computed. This work defines global stability as the stability which is the most critical one (maximum absolute value) among the three. In this work, it was found that 30,000 MC samples are enough for convergence. The value of the mean was used as the convergence criteria. The values of R_{AM}, R_{VM}, R_{FM}, and G against N are shown in Table 1. From Table 1, it is evident that 30,000 samples are sufficient to use in MC simulations. This is because further increasing the number of samples does not change the mean values R_{AM}, R_{VM}, R_{FM}, and G. Thus, convergence is achieved. The bold row indicates that 30,000 samples were used, and the corresponding values obtained using these samples.

TABLE 1 | Values of G against N.

N	R_{AM}	R_{VM}	R_{FM}	G
1000	0.33	0.25	0.25	0.33
5000	0.35	0.26	0.27	0.35
30,000	**0.36**	**0.27**	**0.29**	**0.36**
50,000	0.36	0.27	0.29	0.36
100,000	0.36	0.27	0.29	0.36

To transition from a rigid deterministic security assessment to a realistic probabilistic framework, the operational volatility of both primary energy sources and system consumption must be systematically captured. Wind power generation introduces highly nonlinear uncertainty due to its reliance on stochastic weather patterns. In this framework, the continuous variation of environmental wind speed is represented using an asymmetrical, skewed probability distribution that accurately reflects the localized wind climate, ensuring a realistic representation of periods marked by low wind, rated operational speeds, or high-velocity cutout conditions. Rather than treating wind farm output as a static injection, this model maps the sampled wind speed variations directly to the physical aerodynamic harvesting characteristics of DFIGs. This captures the operational transitions across the cut-in, rated, and cut-out regions, mapping how environmental variations translate into fluctuating electrical active power fed into the grid. Concurrently, system load demand introduces a distinct operational uncertainty governed by aggregate consumer behavior. Unlike the weather-dependent behavior of wind, load volatility is modeled using a symmetrical, bell-shaped probability distribution, centered precisely on the peak

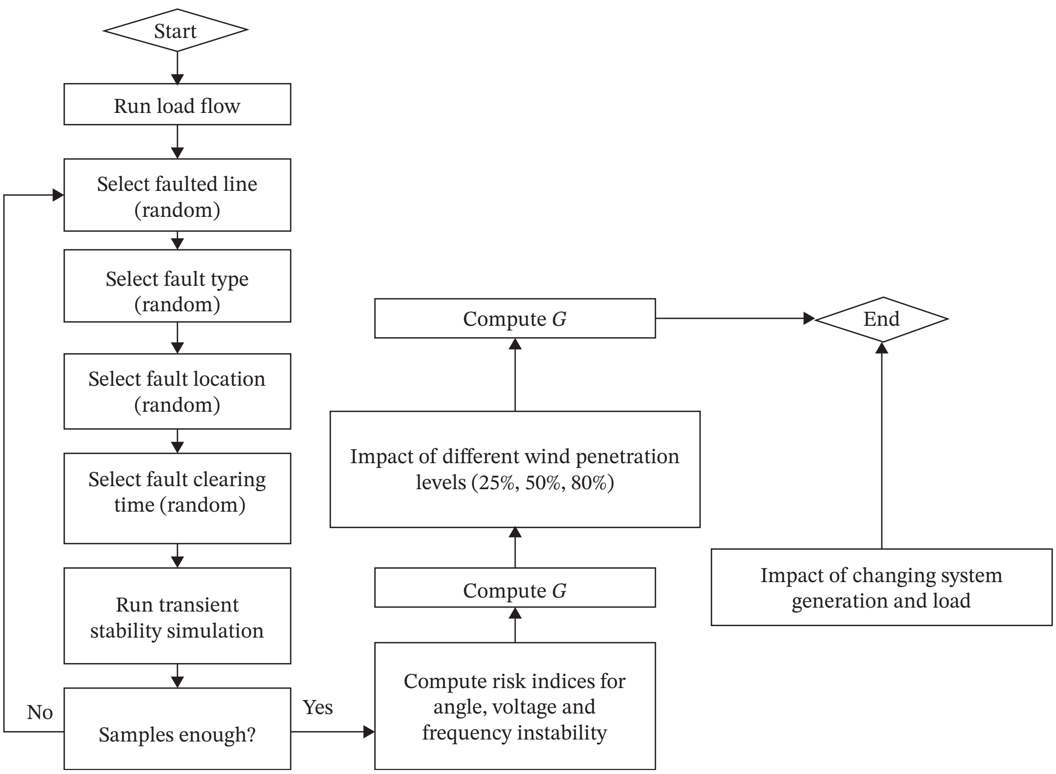

FIGURE 6 | Computation procedure and associated simulations.

forecasted system configuration. This distribution treats the aggregate active and reactive power consumption at each transmission bus as an oscillating variable, allowing for minor and continuous deviations around the baseline demand profile. By overlaying these independent wind and load variations, the pre-fault operational space of the grid is transformed into a multidimensional probability cloud. This configuration serves as the stochastic foundation from which the subsequent contingency analysis randomly samples initial states, capturing the multilayered vulnerabilities of modern power networks.

The proposed probabilistic assessment methodology utilizes a crude MC sampling approach to map the nonlinear propagation of operational uncertainties through the system's differential algebraic equations. This sampling technique is highly robust for large-scale power grids because its statistical convergence rate depends solely on the number of samples rather than the dimension of the stochastic parameter space, avoiding the curse of dimensionality. To balance statistical fidelity with computational efficiency, a total of 30,000 independent operational states and contingency pairings were executed. While extensive time-domain simulations are computationally demanding, the decoupled nature of each MC iteration allows for complete parallelization across high-performance multicore processing environments. This minimizes total execution time, making the methodology highly practical for offline operational planning and the definition of probabilistic dynamic security boundaries.

4 | Modeling of Generation Sources

4.1 | SG

A standard 6^{th} order model is used for modeling all SGs. This model ignores stator and network transients and considers four windings (two on the d-axis and two on the q-axis). All synchronous machines include TGOV1 turbine governor, IEEEX1 exciter, and STAB1 PSS. The mathematical model for a standard 6^{th}-order SG is given by Equations (17)–(22) [45, 48, 49]. It must be mentioned that an extra damping component may be added in Equation (22), if necessary, through a damping torque component which creates a damping torque directly proportional to the rotational speed [49].

$$\mathrm{TJ}\frac{d\omega}{\mathrm{dt}} = \mathrm{M}_m - \mathrm{M}_c - D(\omega - \omega_o). \tag{17}$$

$$\frac{d\delta}{\mathrm{dt}} = \omega - \omega_o. \tag{18}$$

$$T'_{\mathrm{do}}\frac{\mathrm{dE}'_q}{\mathrm{dt}} = E_{\mathrm{fd}} - \left(x_d - x'_d\right)I_d - E'_q. \tag{19}$$

$$T''_{\mathrm{do}}\frac{\mathrm{dE}''_q}{\mathrm{dt}} = -E''_q - \left(x'_d - x''_d\right)I_d + E'_q + T''_{\mathrm{do}}\frac{dE'_q}{d_t}. \tag{20}$$

$$T'_{\mathrm{qo}}\frac{dE'_d}{\mathrm{dt}} = -E'_d + \left(x_q - x'_q\right)I_q. \tag{21}$$

$$T''_{\mathrm{qo}}\frac{dE''_d}{\mathrm{dt}} = -E''_d - \left(x'_q - x''_q\right)I_q + E'_d + T''_{\mathrm{qo}}\frac{dE'_d}{\mathrm{dt}}. \tag{22}$$

4.2 | DFIG

A reduced 3^{rd}-order model, which disregards the stator transients, is used to characterize DFIGs. For power system stability analysis, incorporating the network transients and generator stator transients increases the order of the overall network model, therefore, restricting the network size that can be simulated. Moreover, a small-time step is necessary for numerical integration, resulting in an intensified computational burden. For these purposes, it has become traditional to lower the order of the generator and ignore the network transients for stability analysis. Therefore, the third-order model is the most common DFIG model used to analyze large disturbance stability [50, 51]. The model has a structure like that proposed by the Western Electricity Coordinating Council (WECC) [52] and the International Electrotechnical Commission (IEC) [53]. Disregarding the stator current dynamics, the mathematical equations associated with the DFIG model are given by Equations (23)–(29) [45, 54].

$$\frac{1}{\omega_b}\frac{\mathrm{de}_d}{\mathrm{dt}} = \frac{-1}{T_o}\left[e_d - (X - X')i_{\mathrm{qs}}\right] + s\omega_s e_q - \omega_s\frac{L_m}{L_m + L_r}v_{\mathrm{qr}}. \tag{23}$$

$$\frac{1}{\omega_b}\frac{\mathrm{de}_q}{\mathrm{dt}} = \frac{-1}{T_o}\left[e_q - (X - X')i_{\mathrm{ds}}\right] - s\omega_s e_d + \omega_s\frac{L_m}{L_m + L_r}v_{\mathrm{dr}}. \tag{24}$$

$$\frac{d\omega_r}{\mathrm{dt}} = \frac{1}{2\mathrm{Hg}}\left[K_{\mathrm{tw}}\theta_{\mathrm{tw}} + D_{\mathrm{tw}}(\omega_t - \omega_r) - \left(e_d i_{\mathrm{ds}} + e_q i_{\mathrm{qs}}\right)\right]. \tag{25}$$

$$v_{\mathrm{ds}} = -r_s i_{\mathrm{ds}} + X' i_{\mathrm{qs}} + e_d. \tag{26}$$

$$v_{\mathrm{qs}} = -r_s i_{\mathrm{qs}} - X' i_{\mathrm{ds}} + e_q. \tag{27}$$

$$P_w = v_{\mathrm{ds}}i_{\mathrm{ds}} + v_{\mathrm{qs}}i_{\mathrm{qs}} - v_{\mathrm{dr}}i_{\mathrm{dr}} - v_{\mathrm{qr}}i_{\mathrm{qr}}. \tag{28}$$

$$Q_w = v_{\mathrm{qs}}i_{\mathrm{ds}} - v_{\mathrm{ds}}i_{\mathrm{qs}}. \tag{29}$$

In terms of capabilities of the DFIG wind compared to the SGs, DFIGs can operate at variable rotor speeds, which allows them to use wind resources more efficiently than fixed-speed wind turbines. They can import and export reactive power, which helps stabilize the grid and maintain a consistent electricity supply. They have lower converter costs than other variable-speed solutions as only a small portion of the mechanical power is fed through the converter. They can help reduce mechanical stress and risk of wind turbine failure and can support the grid during severe disturbances. They can decouple the grid power from the mechanical power, which aids in stabilizing the grid faster than a synchronous machine. However, there are some implications of the DFIG limitations compared to those of SG. For instance, DFIGs are sensitive to grid faults, such as sudden short circuits, voltage dips, and swells. These faults can cause stator voltage dips, current oscillations, and torque pulsations. They require maintenance due to the presence of slip rings. The direct connection of the stator to the grid makes the machine more vulnerable to system disturbances. Also, the voltage source converter is a source of harmonics due to switching actions.

5 | Case Studies and Simulations

The 10-machine New England test system (IEEE 39-bus system), operating at 345 kV, was used to perform the required simulations [6]. Pai [55] was used for numerical data and parameters. This system is a reasonable choice for the study as it has been extensively used by numerous academics and researchers for studying the transient stability phenomenon in power systems [56–58]. Also, using this test system can provide fast and accurate assessments, which greatly aid power system planners and operators to understand the dynamics of transient stability. The system one-line diagram is shown in Figure 7. The network consists of 10 SGs, 34 transmission lines, and 12 transformers. It has 19 constant impedance loads totaling 6097.1 MW. The installed capacity of the generators was 6140.81 MW. All wind generators are assumed to be operating at their maximum outputs [45, 59]. Initial operating conditions were based on load flow analysis. Furthermore, it is assumed that the system load is at its peak value. Moreover, the period of transient stability (20 s) makes the variation of load irrelevant as load changes are normally recorded at every 10 or 15-min intervals. All time-domain (dynamic) simulations were RMS simulations, which were conducted with the help of DIgSILENT PowerFactory commercial software [60].

For the practical execution of the stochastic case studies on the modified IEEE 39-bus system, specific physical boundaries were defined to implement the uncertainty models. The environmental wind speed variations across the integrated DFIG–based wind farms were parameterized using a standard wind profile configuration, maintaining a shape parameter that establishes a realistic distribution of wind frequencies and a scale parameter reflecting a robust local wind resource. These speeds map directly into the aerodynamic profiles of the turbines, allowing the generation units to naturally fluctuate between zero output and full capacity based on the simulated atmospheric conditions. Simultaneously, the baseline load demand across all 19 load-bearing buses—which aggregate to a peak system load of 6097.1 MW—was subjected to a structural variation framework. During each iteration of the comprehensive simulation loop, these wind and load parameters are sampled concurrently to reconstruct a

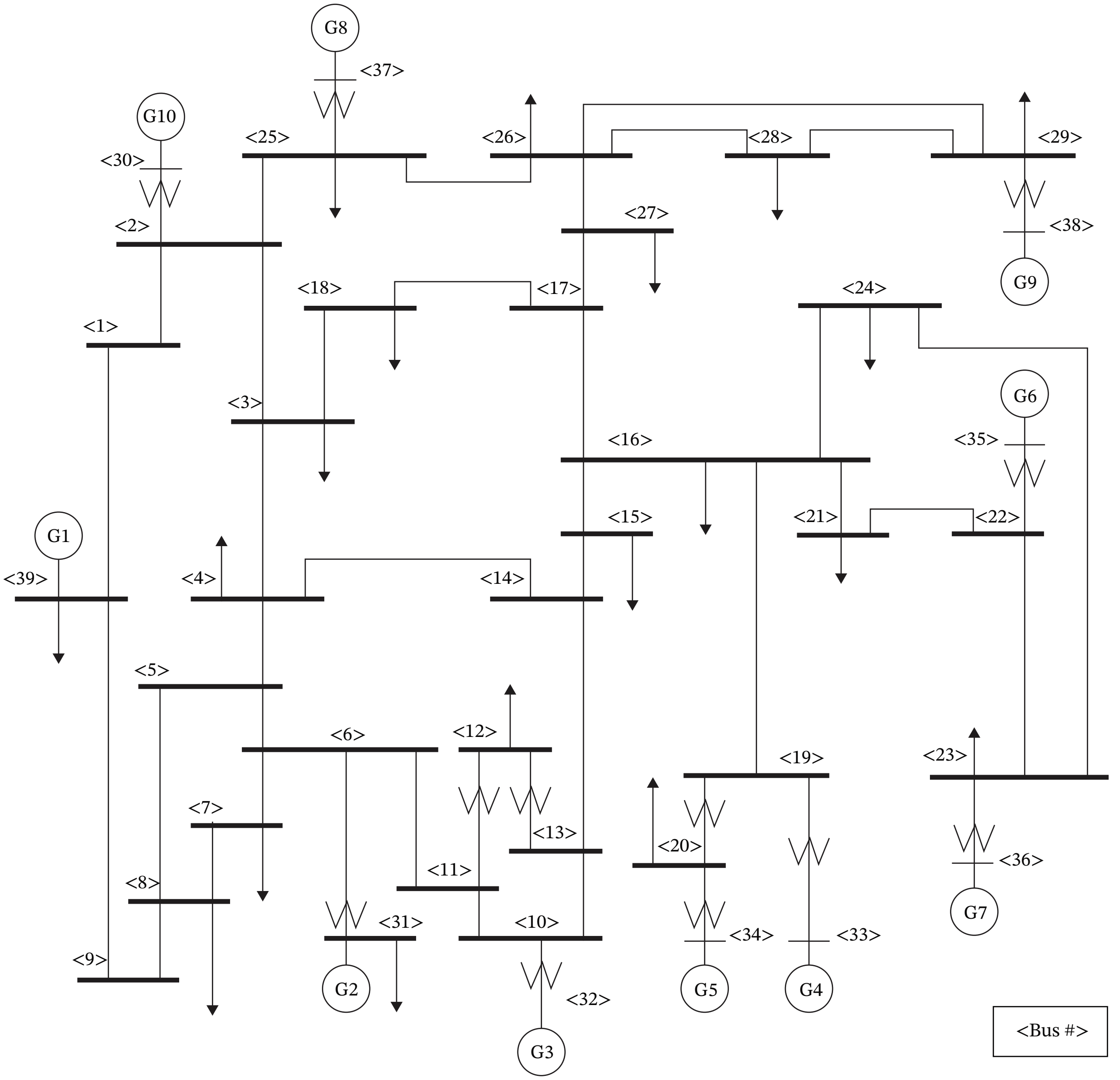

FIGURE 7 | IEEE 39-bus test system.

unique, physically balanced prefault operating point, ensuring that the subsequent severe contingencies test the network across its entire realistic spectrum of operational stress.

6 | Results and Discussion

Based on the computation procedure described in Section 3, values of R_{AM}, R_{VM}, and R_{FM} and eventually G were computed. These values are shown in Table 2. In the next step, synchronous generation was replaced by wind generation, and corresponding values of G were computed. The penetration level in this study is defined as follows:

$$\%\text{Penetration Level} = \frac{\text{Total Renewable Generation (MW)}}{\text{Total System Generation (MW)}} \times 100\%. \tag{30}$$

To reach the necessary penetration levels, specific SGs are substituted by renewable generation sources. Table 3 displays the generators, which were replaced by renewable wind generations to reach the desired penetration level.

For instance, 20% DFIG penetration means that the equivalent amount of synchronous generation (G1 and G10) in the system is replaced by DFIG (with the same MW and MVA rating). A similar process was used to accomplish other penetration levels. Figure 8 shows the value of G for each MC sample. From Figure 8, a distribution can be derived, which is shown in Figure 9 (N_x represents the total number of occurrences). This is a normal (Gaussian) distribution with a mean value of 0.361 and a standard deviation of 0.005. Similar distributions for G are obtained for other cases, as shown in Figures 10–13.

From Figures 10–13, the value of G can easily be computed, that is, the mean values of the corresponding normal distribution obtained. These values are shown in Table 4 and graphically in Figure 14.

TABLE 2 | Values of various risk indices.

Value of various risk indices	SGs replaced
R_{AM}	0.361
R_{VM}	0.336
R_{FM}	0.318
G	0.361

TABLE 3 | Desired DFIG penetration levels.

Desired DFIG penetration level (%)	SGs replaced
20	G1, G10
40	G1, G3, G4, G10
60	G1, G3, G4, G6, G7
80	G1, G4, G5, G6, G8, G9, G10

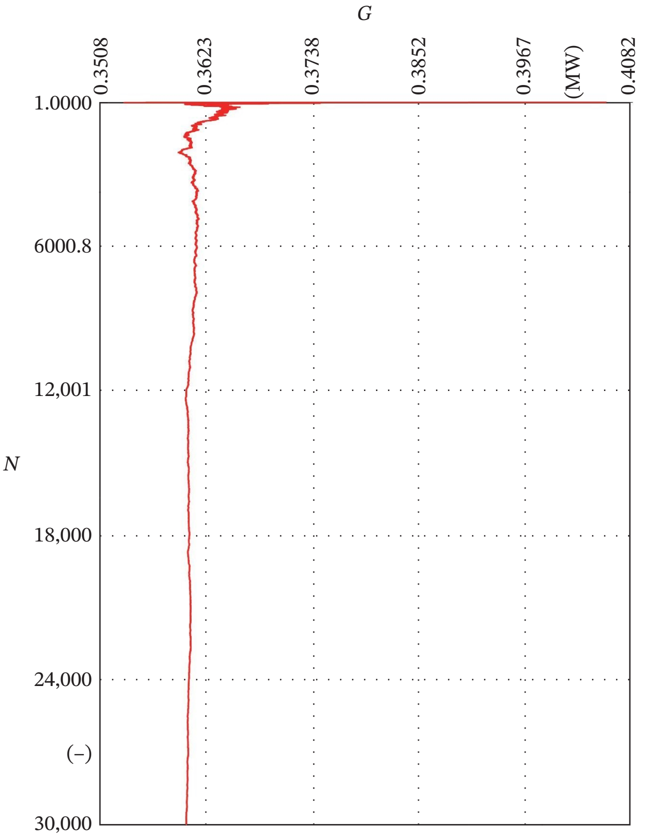

FIGURE 8 | Variation of G with N (base case).

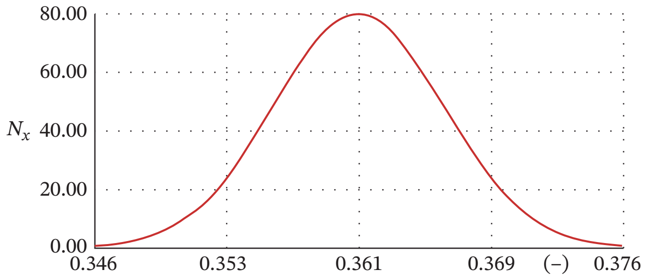

FIGURE 9 | Normal distribution (mean 0.361) of G (base case).

It is evident from Figure 14 that the addition of DFIG in a conventional power system (having only synchronous generation) improves the overall system transient stability. This is because the value of G decreases with increasing wind penetration. A possible reason is the superior reactive power control capabilities of the DFIG during faults. In other words, adding DFIG reduces the probability of the system being unstable as a result of a fault or disturbance. This is because DFIG has the potential to decouple active power management and reactive capacity to improve grid integration (dynamic decoupling). Essentially, a DFIG wind turbine can generate reactive power even when the mechanical part is nonoperating and not delivering active power.

In a nutshell, DFIGs use power electronics to decouple active and reactive power, enabling fast, independent control and voltage support even without wind input. Their variable speed and rapid response improve efficiency and allow quicker system recovery and greater stability than SGs.

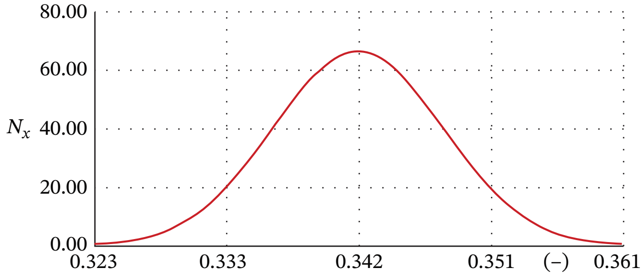

FIGURE 10 | Normal distribution (mean 0.342) of G (20% wind).

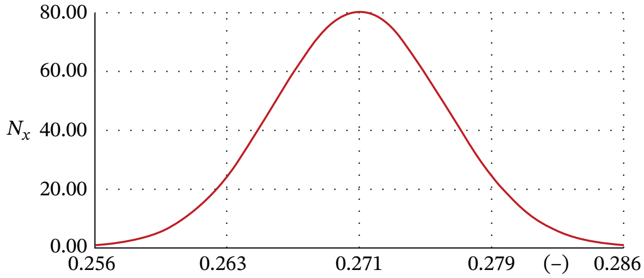

FIGURE 11 | Normal distribution (mean 0.271) of G (40% wind).

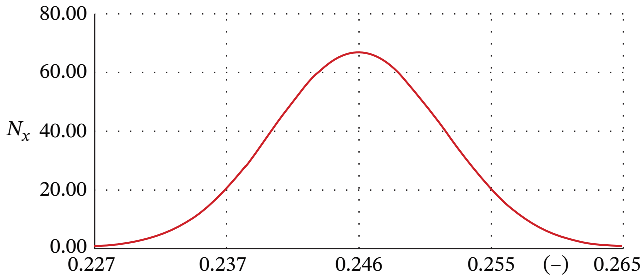

FIGURE 12 | Normal distribution (mean 0.246) of G (60% wind).

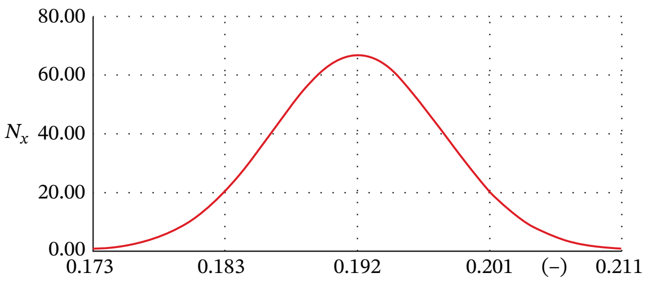

FIGURE 13 | Normal distribution (mean 0.192) of G (80% wind).

It is of great interest to observe the trend of increasing system generation and load on the value of G. Figure 15 shows the impact of increasing system generation (keeping the system load constant) on G. As system generation increases, the value of G starts to decrease. Hence, the system tends to be less risky with respect to stability if system generation is plentiful. However, adding generation is expensive, and care must be taken before doing that. It must be made sure that cost-benefit analysis is conducted before adding a new generation to the system. Figure 16 shows the impact of increasing system load (keeping system generation constant) on G. As system load rises, there is a sharp hike in the value of G. This is understandable as there is no adequate generation to fulfill the system load demand. This makes the system riskier with respect to stability when there is a fault. Hence, the power system operator must exercise caution to assure that critical loss of load does not occur, and if it does occur, it must be restored as quickly as possible.

TABLE 4 | Values of G for different cases.

Case type	G
Base case	0.361
20% wind	0.342
40% wind	0.271
60% wind	0.246
80% wind	0.192

To rigorously demonstrate the necessity of the proposed Global Instability Index, its performance is analytically benchmarked against conventional isolated stability indices under high wind penetration (80%) scenarios. Traditional assessment models analyze risk vectors independently, yielding decoupled risk values for the rotor angle, voltage, and frequency. As observed in the stochastic operational ensembles, under severe contingency profiles, an isolated analysis can generate misleading conclusions. For example, in contingencies where fast-acting DFIG reactive current injection successfully stabilizes local bus voltages post-fault, an independent voltage risk assessment registers an exceptionally low danger index. However, this aggressive converter active/reactive power prioritization temporarily starves the network of primary active power support, exacerbating initial rotor angle swings and frequency nadirs elsewhere in the system.

If an operator monitors these dimensions via an averaged-weighted approach or through isolated indicators, the severe localized risk in the frequency or angular domain is mathematically diluted or overlooked entirely. Conversely, the proposed global index utilizes a nonarbitrary extreme-event formulation. By mapping these physically distinct phenomena into a normalized, dimensionless probability space, the global index ensures that the weakest link in system stability always defines the operational risk margin. The analytical evaluation confirms that while individual metrics underreport composite systemic stress by ignoring cross-domain coupling, the unified framework successfully captures the concurrent vulnerabilities of low-inertia networks, proving to be a highly robust and high-fidelity indicator for modern control centers.

It must be mentioned that the proposed approach has some limitations. For instance, only Type 3 wind generator (DFIG) was used to assess the impact of wind generation on transient instability risk. Only single-line contingencies were considered and the impact of external uncertainties (weather, cyberattacks, human error, etc.) were not considered. The proposed approach can easily encapsulate these limitations, and therefore, provide a good starting point for future studies. It is firmly believed that the presented methodology can greatly promote the improvement of the existing probabilistic methods proposed for power system risk

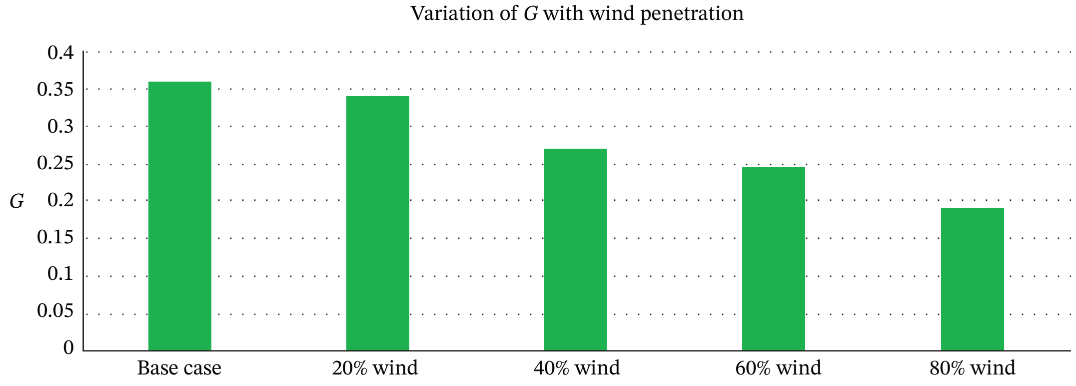

FIGURE 14 | Variation of G with wind penetration.

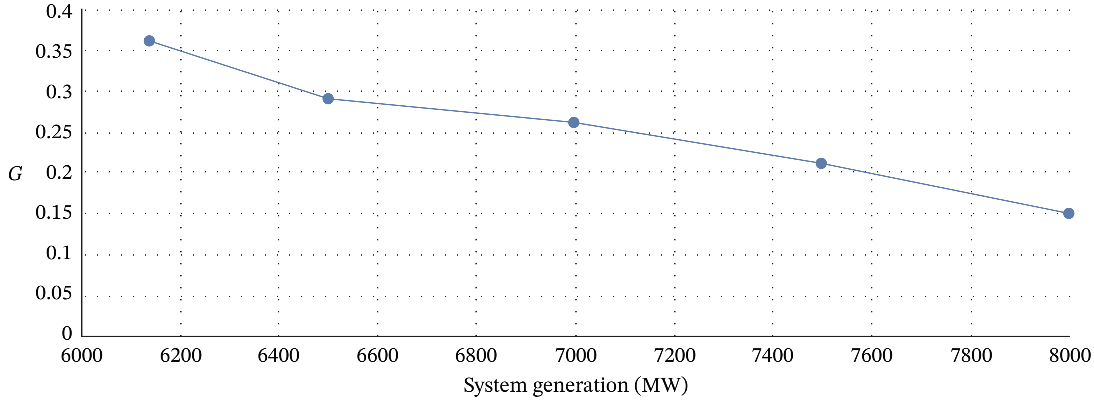

FIGURE 15 | Variation of G with increasing system generation.

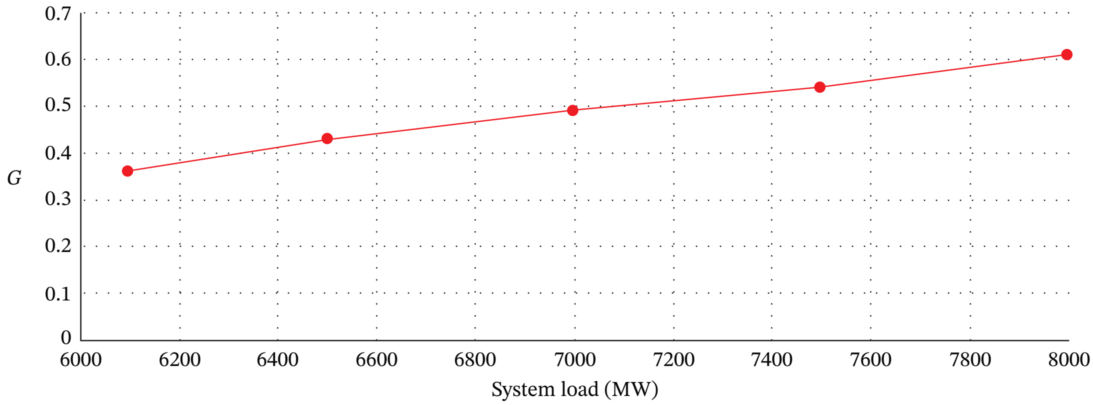

FIGURE 16 | Variation of G with increasing system load.

assessment studies. Various research [45, 47, 61–72] in this domain have signified this challenging issue.

Therefore, to sum up, it is imperative to compute a global instability risk index for a power system. It is not sufficient just to compute a singular stability index. In the case of this paper, angle stability was the most critical, thereby contributing to global instability. Also, it was determined that adding DFIG wind penetration enhances the overall stability of the power system under fault conditions. This is because DFIGs can precisely control the generation of reactive power, which helps stabilize the grid and ensure a consistent electricity supply. They can generate electricity at lower rotational speeds than traditional generators, allowing wind turbines to harness energy even in low wind speeds. They can use the kinetic energy stored in the rotor of the wind turbine to increase the electromagnetic power output of the inverter. This helps slow down frequency drops in a short time.

Also, it was determined that increasing system generation is beneficial for the power system stability. On the contrary, decreasing system load is detrimental to power system stability. It must be mentioned that these findings are not universal and may be different for different test systems under different operating scenarios. However, the approach suggested in this paper can easily be extended to other systems, and consequently, a large number of case studies and simulations can be performed to analyze the behavior of global instability and can be used to form a solid foundation for universal findings. Also, a comparison between the proposed risk-based framework for wind power scenarios can be conducted with other historical samples, including probabilistic hypothesis testing (null and alternative).

To explicitly demonstrate the superiority of the proposed framework, its performance is benchmarked against both traditional ($N-1$) deterministic criteria and standard single-domain probabilistic indices. Conventional deterministic methods evaluate severe contingencies based on rigid, worst-case operational boundaries. In high-penetration wind scenarios (e.g., 80%), these deterministic metrics yield highly conservative and often pessimistic alarms because they cannot account for the statistical likelihood of simultaneous variations. Conversely, while standard probabilistic methods introduce stochastic distributions, they evaluate stability dimensions in strict isolation (e.g., tracking transient stability risk alone), thereby failing to capture multidomain interactions. The proposed Global Instability Index successfully bridges this gap by unifying these fragmented approaches into a single cohesive framework. By mapping rotor angle, voltage, and frequency dimensions into a standardized nonlinear maximum-risk envelope, the proposed framework identifies coupled vulnerabilities—such as a post-fault voltage dip precipitating a frequency nadir—which isolated indices inherently mask. The comparative analysis confirms that the proposed index prevents the dangerous under-reporting or artificial dilution of localized stress, offering transmission operators a high-fidelity, comprehensive representation of true system resilience under high renewable uncertainty.

In terms of practical implementation and usage, the proposed approach can be very helpful for power system planners for making decisions based on risk (probabilistic approach) rather than just considering the conventional approach of using worst case scenarios (deterministic approach), which is less cost efficient. Also, the approach can give power system planners a very good idea of global system stability. Although the worst-case approach has served the power and energy industry well; however, in a competitive environment, the utilities will need to know the level of risk, associated with their observed criteria, such that they adjust their service quality based on the expectation of consumer, that is, the acceptable level of risk and corresponding price. Also, the deterministic approach suffers from various drawbacks. In this approach, only the consequences of contingencies are evaluated, but probabilities of occurrence of contingencies are ignored. Various power system uncertainties (load, renewable generation, electricity price, fault type, fault location, etc.) are ignored in this approach.

In a real-time control room setting, a transmission system operator (TSO) would utilize the *G*-index as a dynamic decision-support tool that moves beyond the limitations of traditional "pass/fail" security checks. How the *G*-index would be integrated into operational workflows is discussed later.

6.1 | Enhanced Situational Awareness and Visualization

Instead of monitoring dozens of separate alarms for voltage, frequency, and rotor angle stability, the TSO can use the *G*-index as a unified "health score" for the grid.

- Heatmaps: The *G*-index can be visualized on a geographic map, where different zones of the IEEE 39-bus (or equivalent real-world grid) are color-coded based on their risk level.
- Trend analysis: Operators can track the *G*-index in real time. A rising trend indicates that while the system is currently "stable" under deterministic rules, the probabilistic risk of a collapse is increasing due to shifting wind patterns or load growth.

6.2 | Proactive Congestion and Resource Management

The paper demonstrates that the *G*-index is sensitive to the load and generation balance. In a control room, this allows for the following:

- Wind dispatch optimization: If the *G*-index rises during peak load, the TSO can utilize the DFIGs' dynamic decoupling and reactive power capabilities. They might choose to curtail older synchronous units in favor of DFIG–based wind farms that, as proven in your study, lower the *G*-index from 0.361 to 0.192.
- Predictive maintenance: TSOs can run "what-if" scenarios. If a specific line needs to be taken out for maintenance, the TSO can calculate the impact on the *G*-index beforehand to ensure that the grid remains within a "low-risk" threshold during the work.

6.3 | Automated Emergency Control Schemes

The *G*-index provides a mathematical basis for system protection schemes (SPSs).

- Dynamic thresholds: Rather than having static load-shedding triggers, the control system can be programmed to trigger preventative actions (like capacitor bank switching or fast-acting frequency response) when the *G*-index exceeds a specific safety margin.
- Risk-based decision making: In a deregulated market, the TSO faces pressure to operate the grid close to its limits for economic efficiency. The *G*-index allows the operator to quantify exactly how much "security" they are sacrificing for "economy," providing a defensible metric for taking expensive out-of-merit actions to maintain system integrity.

7 | Conclusion and Future Work

This research establishes a comprehensive probabilistic framework for evaluating a global instability risk index, *G*, effectively unifying rotor angle, voltage, and frequency stability assessments under the uncertainty of high-capacity wind integration. Validated through MC simulations on the IEEE 39-bus system, the results demonstrate that increasing DFIG penetration from 20% to 80% significantly lowers the system's global risk index from 0.361 to 0.192. This improvement is primarily driven by DFIG's advanced control topologies and dynamic decoupling capabilities, which provide superior reactive power support and grid resilience compared to that of traditional synchronous generation. The significance of the results obtained from stochastic operational testing on the IEEE 39-bus system offers substantial cognitive and practical insights for modern control centers.

Crucially, the quantitative empirical data reveals that a high penetration of DFIG–based wind generation (up to 80%) yields an overall 46.8% reduction in the global instability risk profile. This outcome directly challenges the traditional and conservative paradigm that displacing synchronous generation inherently jeopardizes system resilience. Rather, the analytical results demonstrate that the rapid, decoupled voltage control loops inherent to modern wind energy converters can effectively offset the structural vulnerabilities caused by a reduced kinetic energy buffer. These findings offer vital practical implications for system operators by laying the groundwork for real-time online stability monitoring tools and providing a foundational framework to guide future multi-gigawatt renewable-integrated grid planning.

The study highlights that DFIG–based wind systems provide strong stabilizing effects on power grids, mainly through advanced control features such as synthetic inertia, fast reactive power regulation, and low-voltage ride-through (LVRT). These mechanisms help support frequency and voltage stability during disturbances, prevent premature disconnection of wind farms, and improve overall system resilience under high wind penetration, effectively compensating for the reduced presence of conventional synchronous machines.

However, the current work is limited by its focus on peak wind conditions and does not yet fully address more complex or extreme operating scenarios. Future research will extend the Global Instability Index to include low-wind regimes, grid-forming inverter behavior, and severe multievent disturbances such as $N-2/N-k$ contingencies, generator tripping, and cascading failures. It will also integrate predictive algorithms to track how system risks shift dynamically across angular, voltage, and frequency stability domains during such events.

Moving forward, this universal and scalable framework can be extended to large-scale multiregional power systems to identify localized vulnerabilities and establish hierarchical stability metrics. Future work will also focus on integrating small-signal stability indices and evaluating system performance under complex $(N-k)$ contingencies, such as simultaneous generator and transformer failures. By incorporating a broader range of converter-interfaced resources like solar PV and battery storage, this methodology offers a robust foundation for transitionary grid planning and risk-aware operational decision-making. The framework can be extended to incorporate cyber–physical risks by modeling the impact of false data injection on FCTs and the response of DFIG power electronics. It can also integrate extreme weather effects by replacing uniform fault distributions with weather-dependent fragility models, allowing the G-index to capture real-time environmental hazards and supporting more resilient system operation in climate-volatile conditions.

Nomenclature

i:	i^{th} MC sample
N:	Number of MC samples
$X_{t.f}$:	Forecasted operating condition at time t
$X_{t.j}$:	j^{th} possible loading level
$\Pr(X_{t,j}\|X_t)$:	Probability of $X_{t,j}$ given $X_{t.f}$ has occurred
E_i:	i^{th} contingency
$\Pr(E_i)$:	Probability of i^{th} contingency
$\mathrm{Sev}(E_i, X_{t,j})$:	Impact of E_i occurring under $X_{t,j}$
$R_{\mathrm{A}}(X_{t,f})\ /R_{\mathrm{A}}$:	Risk index for angle instability
$\Pr(F_{\mathrm{oi}})$:	Probability of fault occurrence
$\Pr(F_{\mathrm{Li}})$:	Probability of fault location
$\Pr(F_{\mathrm{Ti}})$:	Probability of fault type
N_L:	Total number of lines in the system
F_i:	i^{th} fault
$\Pr(F_i)$:	Probability of i^{th} fault
$\mathrm{Sev}(A_i, X_{t,j})/\mathrm{Sev}(A_i)$:	Impact of F_i occurring under $X_{t,j}$ (for angle instability)
TSI_i:	Angle stability index for i^{th} MC sample
$\delta_{\mathrm{max}i}$:	Maximum angle difference for i^{th} MC sample
$R_V(X_{t,f})/R_V$:	Risk index for voltage instability
$\mathrm{Sev}(V_i, X_{t,j})/\mathrm{Sev}(V_i)$:	Impact of F_i occurring under $X_{t,j}$ (for voltage instability)
V_{dk}:	Voltage deviation for bus k
V_k:	Postfault steady-state voltage for k^{th} bus
V_{rated}:	Nominal bus voltage
N_b:	Total number of buses in the system
$R_F(X_{t,f})/R_F$:	Risk index for frequency instability
$\mathrm{Sev}(F_i, X_{t,j})$:	Impact of F_i occurring under $X_{t,j}X_{t,j}$ (for frequency instability)
f_{dGk}:	Postfault frequency deviation
N_g:	Total number of generators in the system
R_{AM}:	Mean value of R_{A}
R_{VM}:	Mean value of R_{V}
R_{FM}:	Mean value of R_{F}
R_{An}:	Value of R_{A} for n^{th} MC sample
R_{Vn}:	Value of R_{V} for n^{th} MC sample
R_{Fn}:	Value of R_{F} for n^{th} MC sample
N_x:	Total number of occurrences
G:	Global instability risk index
T_J:	Generator inertia constant
M_m:	Mechanical torque
M_c:	Electromagnetic torque
D:	Damping coefficient
δ:	Rotor angle
ω:	Rotor speed
ω_o:	Synchronous speed
E_{fd}:	Field voltage
E'_d, E'_q:	d- and q-axis components of transient electric potential
E''_d, E''_q:	d- and q-axis components of subtransient electric potential
x_d, x'_d, x''_d:	d-axis synchronous reactance, transient reactance, subtransient reactance

x_q, x_q', x_q'':	q-axis synchronous reactance, transient reactance, subtransient reactance
$T_{\text{do}}', T_{\text{qo}}'$:	d- and q-axis transient time constants
$T_{\text{do}}'', T_{\text{qo}}''$:	d- and q-axis subtransient time constants
P_w:	Active power of DFIG
Q_w:	Reactive power of DFIG
X:	Open-circuit reactance
X':	Short-circuit reactance
K_{tw}:	Shaft stiffness coefficient
D_{tw}:	Mechanical damping coefficient
e_d, e_q:	d and q components of internal voltage
T_o:	Transient open-circuit time constant
H_g:	Generator inertia constant
$\omega_b, \omega_s, \omega_r$:	Base speed, synchronous speed, rotor speed
s:	Generator slip
θ_{tw}:	Shaft twist angle
$v_{\text{ds}}, v_{\text{qs}}$:	Stator voltages
$v_{\text{dr}}, v_{\text{qr}}$:	Rotor voltages
$i_{\text{ds}}, i_{\text{qs}}$:	Stator currents
$i_{\text{dr}}, i_{\text{qr}}$:	Rotor currents
r_s:	Stator resistance
L_m, L_r:	Magnetizing inductance, rotor inductance.

Funding

No funding was received.

Conflicts of Interest

The author declares no conflicts of interest.

Data Availability Statement

The data are available upon request from the author.

References

1. C. P. Steinmetz, "Power Control and Stability of Electric Generating Stations," *Transactions of the American Institute of Electrical Engineers* XXXIX, no. 2 (1920): 1215–1287.

2. AIEE Subcommittee on Interconnections and Stability Factors, "First Report of Power System Stability," *Transactions of the American Institute of Electrical Engineers* 56, no. 2 (1937): 261–282.

3. G. S. Vassell, "Northeast Blackout of 1965," *IEEE Power Engineering Review* 11, no. 1 (1991): 4–8.

4. S. F. B. Shakil, N. Husain, M. D. Wasim, and S. Junaid, "Improving the Voltage Stability and Performance of Power Networks Using Power Electronics Based FACTS Controllers," in *International Conference on Energy Systems and Policies* (2014): 1–6

5. P. Kundur, et al., "Definition and Classification of Power System Stability IEEE/CIGRE Joint Task Force on Stability Terms and Definitions," *IEEE Transactions on Power Systems* 19, no. 3 (2004): 1387–1401.

6. U. Shahzad, "Probabilistic Transient Stability Assessment of Power Systems Using Artificial Neural Network," *Journal of Electrical Engineering, Electronics, Control and Computer Science* 8, no. 1 (2022): 35–42.

7. K. Morison, "Power System Security in the New Market environment: Future Directions," in *IEEE Power and Energy Society Summer Meeting* (2002): 1416-1417

8. M. Mohammadi and G. B. Gharehpeti, "Power System on-Line Static Security Assessment by Using Multi Class Support Vector Machines," *Journal of Applied Sciences* 8, no. 12 (2008): 2226–2233.

9. E. B. Elghali, M. Marsadek, and A. K. Ramasamy, "Risk of Transient Stability Using Rotor Trajectory Index as Severity Function," *Indonesian Journal of Electrical Engineering and Computer Science* 6, no. 3 (2017): 591–601.

10. P. Zhang, K. Meng, and Z. Dong, "Probabilistic Vs Deterministic Power System Stability and Reliability Assessment," in *Emerging Techniques in Power System Analysis*, (Springer, 2010).

11. K. N. Hasan, R. Preece, and J. V. Milanović, "Existing Approaches and Trends in Uncertainty Modelling and Probabilistic Stability Analysis of Power Systems With Renewable Generation," *Renewable and Sustainable Energy Reviews* 101 (2019): 168–180.

12. A. Dissanayaka, U. D. Annakkage, B. Jayasekara, and B. Bagen, "Risk-Based Dynamic Security Assessment," *IEEE Transactions on Power Systems* 26, no. 3 (2011): 1302–1308.

13. W. Li and J. Zhou, "Probabilistic Reliability Assessment of Power System Operations," *Electric Power Components and Systems* 36, no. 10 (2008): 1102–1114.

14. V. E. Van, *Transient Stability Assessment and Decision-Making Using Risk*, (PhD Dissertation, (Iowa State University, USA, 2000).

15. J. V. Milanovic, "Probabilistic Stability Analysis: The Way Forward for Stability Analysis of Sustainable Power Systems," *Philosophical Transactions* 375, no. 2100 (2017): 1–22.

16. W. Li and P. Choudhury, "Probabilistic Planning of Transmission Systems: Why, How and an Actual Example," in *IEEE Power and Energy Society General Meeting —Conversion and Delivery of Electrical Energy in the 21st Century* (2008): 1–8

17. PJM, "PJM Region Transmission Planning Process," 2020, https://www.pjm.com/~/media/documents/manuals/m14b.ashx.

18. Michigan Public Service Commission, "Transmission Planning," 2020, https://www.michigan.gov/documents/mpsc/MPG_Adv_Planning_1.19.21_Presentation_713269_7.pdf.

19. Midwest Reliability Organization, "MRO Regional Risk Assessment," 2024, https://cdn.prod.website-files.com/66d075ffbaf51cf98dfd5bcf/6733acf87e73152fba0d638f_MRO-2024-Regional-Risk-Assessment.pdf.

20. SPP, "Southwest Power Pool," 2020, https://spp.org/documents/62876/spc%20workshop%20materials%202020%2008%2031%20v3.pdf.

21. S. Aboreshaid, "Probabilistic Evaluation of Transient Stability of a Power System Incorporating a UPFC," in *Canadian Conference on Electrical and Computer Engineering* (2003): 441–446

22. M. Al-Sarray, H. Mhiesan, M. Saadeh, and R. McCann, "A Probabilistic Approach for Transient Stability Analysis of Power Systems With Solar Photovoltaic Energy Sources," in *IEEE Green Technologies Conference* (2016): 159–163

23. A. H. Hamida, K. B. Kilani, and M. Elleuch, "Some Aspects of the Tunisian Power System Transient Stability," in *International Multi-Conference on Systems, Signals & Devices* (2017): 383–388

24. P. N. Papadopoulos and J. V. Milanovic, "Probabilistic Framework for Transient Stability Assessment of Power Systems With High Penetration of Renewable Generation," *IEEE Transactions on Power Systems* 32, no. 4 (2017): 3078–3088.

25. J. U. Agber, P. E. Odaba, and C. O. Onah, "Effect of Power System Parameters on Transient Stability Studies," *American Journal of Engineering Research* 4, no. 2 (2015): 87–94.

26. L. Shi, S. Sun, L. Yao, Y. Ni, and M. Bazargan, "Effects of Wind Generation Intermittency and Volatility on Power System Transient Stability," *IET Renewable Power Generation* 8, no. 5 (2014): 509–521.

27. L. Miao, J. Fang, J. Wen, and W. Luo, "Transient Stability Risk Assessment of Power Systems Incorporating Wind Farms," *Journal of Modern Power Systems and Clean Energy* 1, no. 2 (2013): 134–141.

28. Q. Wang, A. Xue, T. Bi, and Y. Zheng, "Impact of DFIG-Based Wind Farm on Transient Stability of Single Machine Infinite Bus System," in *IEEE PES Asia-Pacific Power and Energy Engineering Conference (APPEEC)* (2013): 1–5

29. D. Khani, A. S. Yazdankhah, and H. M. Kojabadi, "Impacts of Distributed Generations on Power System Transient and Voltage Stability," *International Journal of Electrical Power & Energy Systems* 43, no. 1 (2012): 488–500.

30. Z. Zou and K. Zhou, "Voltage Stability of Wind Power Grid Integration," in *International Conference on Electrical Machines and Systems* (2011): 1–5

31. Y. Wang, Y. Sun, and S. Mei, "Modeling of Short-Term Large-Disturbance Voltage Stability Considering Induction Motors," in *2012 IEEE PES Innovative Smart Grid Technologies* (2012): 1–4

32. L. Meegahapola and D. Flynn, "Impact on Transient and Frequency Stability for a Power System at Very High Wind Penetration," in *2010 IEEE PES General Meeting* (2010): 1–8

33. A. Abdlrahem, G. K. Venayagamoorthy, and K. A. Corzine, "Frequency Stability and Control of a Power System With Large PV Plants Using PMU Information," in *2013 North American Power Symposium* (2013): 1–6

34. H. Wan, J. D. McCalley, and V. Vittal, "Risk Based Voltage Security Assessment," *IEEE Transactions on Power Systems* 15, no. 4 (2000): 1247–1254.

35. V. Vittal, J. D. McCalley, V. V. Acker, W. Fu, and N. A. Samra, "Transient Instability Risk Assessment", in *1991 IEEE Power Engineering Society Summer Meeting* (1999): 206–211

36. H. Zhang and Y. Liu, "New Index for Frequency Deviation Security Assessment," in *2010 Conference Proceedings IPEC* (2010): 1031–1034

37. Y. Ma, S. Lv, X. Zhou, and Z. Gao, "Review Analysis of Voltage Stability in Power System," in *2017 IEEE International Conference on Mechatronics and Automation (ICMA)* (2017): 7–12

38. Y. Xue, T. Xu, B. Liu, and Y. Li, "Quantitative Assessments for Transient Voltage Security," *IEEE Transactions on Power Systems* 15, no. 3 (2000): 1077–1083.

39. E. Rakhshani, D. Gusain, V. Sewdien, J. L. Rueda Torres, and M. A. M. M. Van Der Meijden, "A Key Performance Indicator to Assess the Frequency Stability of Wind Generation Dominated Power System," *IEEE Access* 7 (2019): 130957–130969.

40. J. Fang, H. Li, Y. Tang, and F. Blaabjerg, "On the Inertia of Future More-Electronics Power Systems," *IEEE Journal of Emerging and Selected Topics in Power Electronics* 7, no. 4 (2019): 2130–2146.

41. U. Shahzad, "A Probabilistic Framework for Power System Large-Disturbance Global Instability Risk Assessment in the Presence of Renewable Wind Generation," 2022, https://arxiv.org/abs/2205.03629.

42. D. H. Nguyen and M. Negnevitsky, "A probabilistic Approach for Power System Security Assessment," in *2012 Australasian Universities Power Engineering Conference (AUPEC)* (2012): 1–6

43. C. Li, L. Jing, and C. Jing, "Research of Risk-Based Security Assessment of Power System," in *2011 International Conference on Electric Utility Deregulation and Restructuring and Power Technologies (DRPT)* (2011): 1335–1340

44. U. Shahzad and S. Asgarpoor, "Probabilistic Evaluation of Line Loading and Line Active Power in an Active Distribution Network Using Numerical and Analytical Approaches," in *2018 North American Power Symposium* (2018): 1–6

45. U. Shahzad, "Impact of Renewable Generation on Probabilistic Dynamic Security Assessment of a Power Transmission System," *Australian Journal of Electrical and Electronics Engineering* 18, no. 3 (2021): 181–191.

46. M. Abapour and M.-R. Haghifam, "Probabilistic Transient Stability Assessment for on-Line Applications," *International Journal of Electrical Power & Energy Systems* 42, no. 1 (2012): 627–634.

47. U. Shahzad, "Application of Supervised Machine Learning for Prediction of Probabilistic Transient Stability," *Australian Journal of Electrical and Electronics Engineering* 19, no. 1 (2022): 65–78.

48. Y. N. Zhu and J. X. Jin, "Simulation Analysis of a Synchronous Generator System Under Fault Conditions," in *2013 IEEE International Conference on Applied Superconductivity and Electromagnetic Devices* (2013): 180–184

49. T. Weckesser, H. Jóhannsson, and J. Østergaard, "Impact of Model Detail of Synchronous Machines on Real-Time Transient Stability Assessment," in *2013 IREP Symposium Bulk Power System Dynamics and Control - IX Optimization, Security and Control of the Emerging Power Grid* (2013): 1–9

50. M. Atallah, "Modeling and Power Control of 5th and 3rd Order Model for DFIG Applied of Wind Conversion System," *International Journal of Energetica* 6, no. 2 (2021): 44–51.

51. J. B. Ekanayake, L. Holdsworth, and N. Jenkins, "Comparison of 5th Order and 3rd Order Machine Models for Doubly Fed Induction Generator (DFIG) Wind Turbines," *Electric Power Systems Research* 67, no. 3 (2003): 207–215.

52. WECC, "WECC Wind Power Plant Dynamic Modeling Guide, WECC Renewable Energy Modeling Task Force," 2014, https://www.wecc.org/sites/default/files/documents/meeting/2024/WECC%20Wind%20Plant%20Dynamic%20Modeling%20Guidelines.pdf.

53. IEC, "Wind Turbines - Part 27-1: Electrical Simulation Models—Wind Turbines," 2015, IEC. 61400-27-1 https://infostore.saiglobal.com/preview/is/en/2015/i.s.en61400-27-1-2015.pdf?sku=1841002.

54. S. Xia, Q. Zhang, S. T. Hussain, B. Hong, and W. Zou, "Impacts of Integration of Wind Farms on Power System Transient Stability," *Applied Sciences* 8, no. 8 (2018): 1289.

55. M. A. Pai, *Energy Function Analysis for Power System Stability*, 1st ed. (Kluwer, 1989, https://webstore.iec.ch/en/iec_catalog/product/preview/?id=L3AtcHViL3ByZXZpZXcvaW5mb19pZWM2MTQwMC0yNy0xe2VkMS4wfWIucGRm.

56. P. Bhui and N. Senroy, "Real-Time Prediction and Control of Transient Stability Using Transient Energy Function," *IEEE Transactions on Power Systems* 32, no. 2 (2017): 923–934.

57. L. Tang and W. Sun, "An Automated Transient Stability Constrained Optimal Power Flow Based on Trajectory Sensitivity Analysis," *IEEE Transactions on Power Systems* 32, no. 1 (2017): 590–599.

58. D. R. Gurusinghe and A. D. Rajapakse, "Post-Disturbance Transient Stability Status Prediction Using Synchrophasor Measurements," *IEEE Transactions on Power Systems* 31, no. 5 (2016): 3656–3664.

59. L. Meegahapola, D. Flynn, and T. Littler, "Transient Stability Analysis of a Power System With High Wind Penetration," in *2008 International Universities Power Engineering Conference* (2008): 1–5

60. DIgSILENT GmbH, "DIgSILENT PowerFactory User Manual," (2018).

61. U. Shahzad, "Transient Stability Risk Assessment Framework Incorporating Circuit Breaker Failure and Severe Weather," *Australian Journal of Electrical and Electronics Engineering* 19, no. 2 (2022): 137–148.

62. C. Lin, F. Liu, L. Zhang, G. Li, C. Chen, and Z. Bie, "An Online Data-Driven Risk Assessment Method for Resilient Distribution Systems,"

CPSS Transactions on Power Electronics and Applications 6, no. 2 (2021): 136–144.

63. C. Pan, B. Hu, C. Shao, H. Lu, K. Xie, and A. Anvari-Moghaddam, “Modelling Supply-Demand Imbalance Risk in Power Systems With Wind Power Reserves,” in *2023 IEEE Sustainable Power and Energy Conference* (2023): 1–6

64. Y. Wang, Y. Li, T. Xu, and M. Zhu, “Cascading Failure Risk Assessment Based on Event-Driven Model in a Cyber-Physical Power System,” in *2023 IEEE International Conference on Power Science and Technology (ICPST)* (2023): 123–128

65. K. Yan, X. Liu, Y. Lu, and F. Qin, “A Cyber-Physical Power System Risk Assessment Model Against Cyberattacks,” *IEEE Systems Journal* 17, no. 2 (2023): 2018–2028.

66. Z. Ding, K. Yu, C. Wang, and W.-J. Lee, “Transmission Line Overload Risk Assessment Considering Dynamic Line Rating Mechanism in a High-Wind-Penetrated Power System: A Data-Driven Approach,” *IEEE Transactions on Sustainable Energy* 13, no. 2 (2022): 1112–1122.

67. D. You, S. Gao, and X. Chen, “Incremental Learning-Based Online Risk Assessment of Power System Operation With High Renewable Energy Penetration,” in *2023 IEEE Sustainable Power and Energy Conference* (2023): 1–6

68. T. Dai, C. Yang, C. Xu, and J. Meng, “An Artificial Intelligence-Based Security Risk Assessment Model for Power Systems,” in *Asia Conference on Energy Conversion Systems and Power Electronics (AECSPE)* (2025): 258–262

69. X. Hu, X. Wang, P. Li, and Y. Chen, “Risk Assessment of Cascading Failures in Power Systems and Vulnerability Aanalysis of Key Lines,” in *2025 4th Asia Power and Electrical Technology Conference (APET)* (2025): 707–711

70. T. Chen, Z. Zou, Y. Hu, and Y. Teng, “Research on Dynamic Risk Assessment Methods for the New Power System Based on Deep Reinforcement Learning,” in *8th Advanced Information Technology, Electronic and Automation Control Conference (IAEAC)*, (IEEE, 2025): 411–416.

71. U. Shahzad, “A Probabilistic Framework for Power System Large-Disturbance Global Instability Risk Assessment in the Presence of Renewable Wind Generation,” arXiv preprint arXiv: 2205.03629 (2022).

72. U. Shahzad, *Risk-Based Machine Learning Approaches for Probabilistic Transient Stability*, (Ph.D. dissertation https://digitalcommons.unl.edu/elecengtheses/148/, (University of Nebraska-Lincoln, Lincoln, NE, USA, 2021).

Author Biographies

Dr. Umair Shahzad is currently a Lecturer at the School of Computer Science and Engineering, University of Sunderland, UK. He received his Ph.D. in Electrical Engineering from the University of Nebraska–Lincoln (USA) in 2021, where his research focused on risk-based machine learning approaches for power system probabilistic transient stability. The results of his Ph.D. research have been widely published and cited in numerous high-impact journals and leading conferences. He earned a B.Sc. in Electrical Engineering from University of Engineering and Technology, Lahore, in 2010 and an M.Sc. in Electrical Engineering from the University of Nottingham (UK) in 2012. Additionally, he holds a Postgraduate Certificate in Education (PGCE) from the University of Sunderland, UK. His research interests include power system security assessment, power system stability, artificial intelligence, machine learning, and probabilistic methods applied to power systems.